Received: 8 January 2020 | Revised: 13 February 2020 | Accepted: 14 February 2020

DOI: 10.1002/mdp2.163

WILEY

SPECIAL ISSUE ARTICLE

Numerical simulation of high-velocity impact on fiber-reinforced composites using MAT_162

R. Scazzosi | **M. Giglio** | **A. Manes**

Dipartimento di Meccanica, Politecnico di Milano, Milan, Italy

Correspondence
Riccardo Scazzosi, Dipartimento di Meccanica, Politecnico di Milano, Via La Masa 1, Milan 20156, Italy.
Email: riccardo.scazzosi@polimi.it

Abstract

MAT_162 is an enhanced material model for fiber-reinforced composites implemented in the software LS-DYNA, which considers different failure modes in tension, compression, and shear, with a progressive failure model. It takes into account the strain rate sensitivity of the strength and moduli properties using a logarithmic function. This material model is commonly used in the literature for modeling glass fiber-reinforced composites while only a few studies related to aramid fiber-reinforced composites can be found. Aramid fibers are one of the most common fibers used in the manufacturing of ballistic shields due to their excellent mechanical properties. The scope of this study is to evaluate the accuracy of the material model MAT_162 in simulating high-velocity impact on aramid fiber-reinforced composites. An actual .357 Magnum projectile is impacted at different velocities, and therefore, different scenarios from the arrest of the projectile to the full penetration of the target are considered. MAT_162 is compared with MAT_058, which is a simpler material model that needs less input material parameters and is therefore easier to be implemented. Finally, parametric studies and a mesh convergence analysis are performed.

KEYWORDS

composites, composite laminates, fiber-reinforced composite, finite element, finite element method, high-velocity impact, numerical simulation, numerical modeling

1 | INTRODUCTION

Ballistic shields are used whenever protection from external threats is required. Fiber-reinforced composites are a preferred choice for the manufacturing of ballistic shields for vehicles, where lightweight solutions are preferred to reduce fuel consumption or increase payload, because they have a favorable combination of high strength and low density. Aramid fibers are a common choice when high tensile strength and resistance to impact damage are required,[1] together with reduced weight and a reasonable cost. High-velocity impact on aramid fiber-reinforced composites is usually modeled using a macroscale approach where the material is considered as an equivalent homogenous medium, with no distinction between the fibers and the matrix, with orthotropic mechanical properties.[2-11]

Composite MSC (MAT_161 and MAT_162) is an enhanced material model for fiber-reinforced composites developed by Material Science Corporation and implemented in the software LS-DYNA, which considers different failure modes in tension, compression, and shear with a progressive failure model. It takes into account the strain rate sensitivity of the strength and moduli properties using a logarithmic function.[12] However, 34 input parameters are necessary

for its implementation.[13] Several studies are present in the literature where the material model is implemented for modeling glass fiber-reinforced composites,[13-17] while only few studies related to aramid fiber-reinforced composites can be found. In some studies,[5,18] the material model MAT_162 is used for the simulation of high-velocity impact on a combat helmet, which is manufactured from aramid fiber-reinforced composites, but these studies focus only on the case of a projectile arrest without partial or full penetration of the target.

The scope of this study is to evaluate the accuracy of the material model MAT_162 in simulating high-velocity impact on aramid fiber-reinforced composites. MAT_162 is chosen since it is a generalization of MAT_161. A .357 Magnum projectile is impacted at different velocities, and therefore, different scenarios from the arrest of the projectile to the full penetration of the target are considered. MAT_162 is compared with laminated composite fabric (MAT_058), which is a simpler material model that needs less input materials parameters and is therefore easier to be implemented. The outcomes of the model simulations are compared with experimental results already obtained by the authors in Scazzosi et al[19] where an innovative analytical model for high-velocity impact on fiber-reinforced composites was developed. Furthermore, parametric studies and mesh convergence analysis are performed and reported in the present article. In Section 2, the numerical models are described while the results of the simulation are discussed in Section 3. Finally, conclusions are drawn in Section 4.

2 | NUMERICAL MODEL

The numerical models developed are aimed at simulating the high-velocity impact test already performed by the authors for the validation of a new analytical model.[19] In these experimental tests, a. 357 Magnum bullet was shot at composite panels made of 14 layers of plain weave Kevlar 29 embedded in an epoxy matrix. This material has already been characterized by the authors by means of tensile tests[7]: The elastic modulus was 10.06 $\pm$ 0.65 GPa (calculated in the strain range between 1.8 and 2.2%), and the tensile strength was 405.24 $\pm$ 18.03 MPa. The bullet was shot at different impact velocities ranging from 700 to 300 m/s to obtain the ballistic curve. For a more detailed description of the experimental tests, the reader is referred to Scazzosi et al.[19]

The two numerical models developed (see Figure 1), laminated composite fabric (MAT_058) and composite MSC (MAT_162), were identical except for the material model used for the composite and for the mesh of the composite panel, since the two material models adopted require different element types. The numerical models were three-dimensional, and double symmetry of the problem was exploited to decrease the computational time.[3,4,6-9] This means that only a quarter of the geometry was modeled and that suitable symmetry conditions were applied. The projectile was a conical tip soft core bullet with a lead core and a brass jacket. The two components of the bullet were modeled as separate entities using constant-stress solid element with complete integration. During the experimental tests, it was noticed that the jacket was not ripped off during the impact but remained attached to the core. For this reason, a

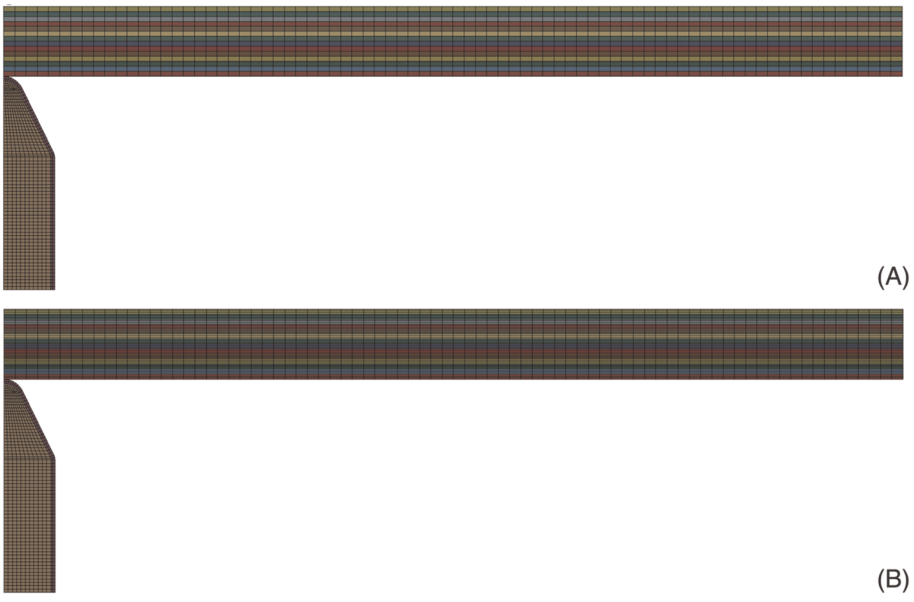

FIGURE 1 Numerical model for A, MAT_058 and B, MAT_162 (composite layers represented with different colors)

TIED_SURFACE_TO_SURFACE contact was used to avoid relative motion between the nodes of the contact surfaces of the two parts. ERODING_SURFACE_TO_SURFACE contact was used between the bullet and the target, and the friction coefficient was set to 0.27.[20] The materials of the bullet were modeled using the material model modified Johnson-Cook with Cockcroft-Latham failure criterion (MAT_107). The input parameters are reported in Table 1. E and ν are respectively the elastic modulus and the Poisson's ratio; A, B, and n are the Johnson-Cook strain hardening parameters; C is the strain rate sensitivity parameter; $\dot{\epsilon}_0$ the reference strain rate; m is the thermal softening parameter; T_m is the melting temperature; and W_{cr} is the Cockcroft-Latham parameter. The parameter C was obtained by fitting the modified Johnson-Cook equation for strain rate sensitivity with the Johnson-Cook equation used in the original reference (Gilioli et al[21] and Zukas[22] for lead and brass, respectively). The target was a composite panel, which was modeled as a quarter of 80 × 80 mm and a thickness of 6.5 mm.[19] The mesh is described in Sections 2.1 and 2.2 since it depends on the material model used. Encastre boundary conditions were applied to the outer edges to model the effect of the fixing frame.

2.1 | MAT_058: Laminated composite fabrics

Matzenmiller, Lubliner, and Taylor developed a constitutive model for anisotropic damage in fiber-reinforced composites,[23] which is implemented in laminated composite fabrics material model (MAT_058). The material model is suitable for both unidirectional fiber-reinforced composites and woven fabrics composites. Here, the material model with a smooth failure surface denoted as material 58b (chosen by selecting FS = 1 in the material card) is described since it is the one adopted in this study.[24] The failure criterion is the same in the 11- and 22-direction as defined in Equations (1) and (2).

$$f_{11} = \frac{\sigma_{11}^2}{(1-\omega_{11c,t})^2 X_{c,t}^2} + \frac{\tau^2}{(1-\omega_{12})^2 S_c^2} - r_{\|c,t} = 0, \tag{1}$$

$$f_{22} = \frac{\sigma_{22}^2}{(1-\omega_{22c,t})^2 Y_{c,t}^2} + \frac{\tau^2}{(1-\omega_{12})^2 S_c^2} - r_{\|c,t} = 0, \tag{2}$$

where $X_{c,t}$, $Y_{c,t}$, and S_c are the material strengths, as described in Table 2, and ω is a damage parameter that is different in tension and in compression for the 11- and 22-direction, in order to account for one-sidedness, which is typical in many materials, while it does not depend on the shear direction (12-direction). The reader is referred to Schweizerhof et al[24] for the description of the damage model. The damage evolution is modified such that the stress does not fall below a threshold value, which is defined by the parameter called SLIMxx equal to the ratio between the threshold value (σ_{min}) and the strength as defined in Equation (3).[25]

TABLE 1 MAT_107 input parameters for the lead core and brass jacket

Material	Lead	Brass
E (MPa)	16 000[21]	115 000[29]
ν	0.42[21]	0.31[29]
A (MPa)	0[21]	111.69[22]
B	55.552[21]	504.69[22]
n	0.0987[21]	0.42[22]
$\dot{\epsilon}_0$ (s^{-1})	72.108[21]	1[22]
C	0.126	0.0085
T_m (K)	525[21]	1189[29]
m	1[21]	1.68[22]
W_{cr} (MPa)	175[29]	914[29]

TABLE 2 MAT_058 input parameters for Kevlar29/epoxy

Symbol	Property	Value
ρ	Density	1025 kg/m3[7]
E_a	Elastic modulus 1	10.06 GPa[7]
E_b	Elastic modulus 2	10.06 GPa[7]
E_c	Elastic modulus 3	6 GPa[6]
ν_{ba}	Poisson's ratio 21	0.25[6]
ν_{ca}	Poisson's ratio 31	0.33[6]
ν_{cb}	Poisson's ratio 32	0.33[6]
G_{ab}	Shear modulus 12	0.77 GPa[6]
G_{bc}	Shear modulus 23	5.43 GPa[6]
G_{ca}	Shear modulus 31	5.43 GPa[6]
X_t	Tensile strength 1	Defined as a function of the strain rate (see Figure 2A)
Y_t	Tensile strength 2	Defined as a function of the strain rate (see Figure 2A)
X_c	Compressive strength 1	Defined as a function of the strain rate (see Figure 2B)
Y_c	Compressive strength 2	Defined as a function of the strain rate (see Figure 2B)
S_c	Shear strength 12 plane	77 MPa[6]
SLIMT1	Factor to determine the minimum stress limit (tension 1)	0.1
SLIMT2	Factor to determine the minimum stress limit (tension 2)	0.1
SLIMC1	Factor to determine the minimum stress limit (compression 1)	1
SLIMC2	Factor to determine minimum stress limit (compression 2)	1
SLIMS	Factor to determine minimum stress limit (shear)	1
ERODS	Maximum effective strain for element erosion	1

$$\sigma_{\min} = SLIM_{xx} \cdot strength \tag{3}$$

The user can thus define different threshold values for the 11- and 22-direction in tension and compression (respectively SLIMT1, SLIMC1, SLIMT2, and SLIMC2) and in the 12-direction (SLIMS). A small value for tensile failure (SLIMT1 and SLIMT2) is usually preferred, between 0.05 and 0.1, while a value of 1 is usually preferred in compression (SLIMC1 and SLIMC2) and shear (SLIMS).[25]

The values of X_t, Y_t, X_c, and Y_c were defined as a function of strain rate by means of tabular data. The relation that describes the value of the strength function of the strain rate is defined in Equation (4) (which is the same function used in MAT_162).

$$\sigma = \sigma_0 \left[1 + C_{\text{rate1}} ln\left(\frac{\dot{\epsilon}}{\dot{\epsilon}_0}\right)\right], \tag{4}$$

where σ is the strength at the strain rate $\dot{\epsilon}$, σ_0 is the static strength, $C_{\text{rate1}} = 0.0257$,[5] and $\dot{\epsilon}_0 = 1\ s^{-1}$ to be consistent with MAT_162. In both the 11- and 22-direction, the static strength in tension is 405 MPa[7] while the compressive strength is 185 MPa.[6] The curves obtained by means of Equation (4) and given as an input to the software are shown in Figure 2.

ERODS is the maximum effective strain for element erosion, which is necessary to remove overstrained elements from the model. This value must be chosen so that it does not affect the failure criterion and that the model is not polluted by overstrained elements.[26]

The material input parameters for Kevlar29/epoxy are reported in Table 2.

Since MAT_058 is implemented only for shell and thick shell elements, each layer of the panel is modeled as a separate entity. Only one thick shell element trough the thickness of each layer was used (see Figure 1A). The dimensions of the elements were 1 × 1 × 0.445 mm where 0.445 mm is the average thickness of the layers. AUTOMATIC_SURFACE_TO_SURFACE_TIEBREAK is the contact algorithm used to model the interaction between

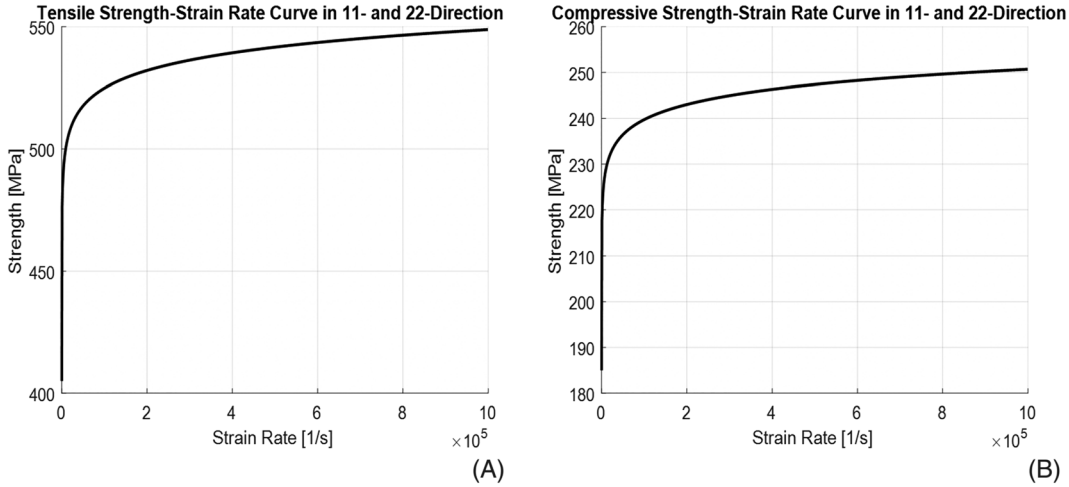

FIGURE 2 Strength-strain rate curve in 11- and 22- direction in A, tension and B, compression

the layers. In this algorithm, the nodes that lie on the faces at the interface between two adjacent layers are tied until the interface failure criterion is satisfied. This is defined by Equation (5):

$$\left(\frac{\sigma_n}{S_n}\right)^2 + \left(\frac{\tau}{S_s}\right)^2 - 1 \geq 0, \tag{5}$$

where S_n is the interfacial normal stress threshold and S_s is the interfacial shear stress threshold, which were respectively 34.5 and 9 MPa.[6]

2.2 | MAT_162: Composite MSC

The material model composite MSC (MAT_161 and MAT_162) is implemented to model either unidirectional or woven fabric composites. In particular, MAT_162 was used in this study, which is a generalization of MAT_161 and adopts the damage mechanic approach of Matzenmiller, Lubliner, and Taylor.[23] Here, the material model for woven fabrics is described (chosen by selecting AMODEL = 2 in the material card) since it is the one adopted in this study. The material model implies seven failure criteria. The tension-shear fiber mode failures are defined in Equations (6) and (7):

$$f_7 - r_7^2 = \left(\frac{E_a\langle\epsilon_1\rangle}{S_{aT}}\right)^2 + \left(\frac{G_{ca}\epsilon_{31}}{S_{aFS}}\right)^2 - r_7^2, \tag{6}$$

$$f_8 - r_8^2 = \left(\frac{E_b\langle\epsilon_2\rangle}{S_{bT}}\right)^2 + \left(\frac{G_{bc}\epsilon_{23}}{S_{bFS}}\right)^2 - r_7^2, \tag{7}$$

where E_a, E_b, G_{ca}, G_{bc}, S_{aT}, S_{bT}, and SFS are the material input parameters as defined in Table 3, $S_{aFS} = S_{FS}$ and $S_{bFS} = S_{FS}xS_{bT}/S_{aT}$.

The compression fiber mode failures are defined in Equations (8) and (9):

$$f_9 - r_9^2 = \left[\frac{E_a\left(-\epsilon_1 - \langle\epsilon_3\rangle\frac{E_c}{E_a}\right)}{S_{aC}}\right]^2 - r_9^2, \tag{8}$$

TABLE 3 MAT_162 input parameters for Kevlar29/epoxy

Symbol	Property	Value
ρ	Density	1025 kg/m3[7]
E_a	Elastic modulus 1	10.06 GPa[7]
E_b	Elastic modulus 2	10.06 GPa[7]
E_c	Elastic modulus 3	6 GPa[6]
ν_{ba}	Poisson's ratio 21	0.25[6]
ν_{ca}	Poisson's ratio 31	0.33[6]
ν_{cb}	Poisson's ratio 32	0.33[6]
G_{ab}	Shear modulus 12	0.77 GPa[6]
G_{bc}	Shear modulus 23	5.43 GPa[6]
G_{ca}	Shear modulus 31	5.43 GPa[6]
S_{aT}	Tensile strength 1	405 MPa[7]
S_{aC}	Compressive strength 1	185 MPa[6]
S_{bT}	Tensile strength 2	405 MPa[7]
S_{bC}	Compressive strength 2	185 MPa[6]
S_{cT}	Through thickness tensile strength	34.5 MPa[5]
S_{FC}	Crush strength	1200 MPa[5]
S_{FS}	Fiber mode shear strength	1086 MPa[5]
S_{AB}	Matrix mode shear strength plane 12	77 MPa[5]
S_{BC}	Matrix mode shear strength plane 23	898 MPa[5]
S_{CA}	Matrix mode shear strength plane 31	898 MPa[5]
S_{FFC}	Scale factor for residual compressive strength	0.3[5]
ϕ	Coulomb's friction angle	10°[5]
E_LIMT	Element eroding axial strain	4.5[5]
S	Scale factor for the delamination criterion	1.2[5]
OMGMX	Limit damage parameter for the elastic modulus reduction	0.9975[5]
ECRSH	Limit compressive relative volume for the element eroding	0.001[5]
EEXPN	Limit tensile relative volume for the element eroding	5[5]
AM1	Coefficient for the strain softening property	0.5[5]
AM2	Coefficient for the strain softening property	0.5[5]
AM3	Coefficient for the strain softening property	1[5]
AM4	Coefficient for the strain softening property	20[5]
C_{rate1}	Coefficient for the strain rate dependence	0.0257[5]
C_{rate2}	Coefficient for the strain rate dependence	0.0246[5]
C_{rate3}	Coefficient for the strain rate dependence	0.0246[5]
C_{rate4}	Coefficient for the strain rate dependence	0[5]

$$f_{10} - r_{10}^2 = \left[\frac{E_b\left(-\epsilon_2 - \langle\epsilon_3\rangle\frac{E_c}{E_b}\right)}{S_{bC}}\right]^2 - r_{10}^2, \tag{9}$$

where E_c, S_{aC}, and S_{bC} are the material input parameters as defined in Table 3.

The crush mode failure is defined in Equation (10):

$$f_{11} - r_{11}^2 = \left(\frac{E_c\langle -\epsilon_3\rangle}{S_{FC}}\right)^2 - r_{11}^2, \tag{10}$$

where S_{FC} is a material input parameter as defined in Table 3.

The in-plane matrix mode failure is defined in Equation (11):

$$f_{12} - r_{12}^2 = \left(\frac{G_{ab}\langle \epsilon_{12}\rangle}{S_{ab}}\right)^2 - r_{12}^2, \tag{11}$$

where G_{ab} and S_{ab} are the material input parameters as defined in Table 3.

The parallel matrix mode failure (delamination) is defined in Equation (12):

$$f_{13} - r_{13}^2 = S^2\left\{\left(\frac{E_c\langle \epsilon_3\rangle}{S_{cT}}\right)^2 + \left(\frac{G_{bc}\epsilon_{23}}{S_{bc0} + S_{SRC}}\right)^2 + \left(\frac{G_{ca}\epsilon_{31}}{S_{ca0} + S_{SRC}}\right)^2\right\} - r_{13}^2, \tag{12}$$

where S_{cT}, S_{bc0}, and S_{ca0} are the material input parameters as defined in Table 3. S_{SRC} is defined as

$$S_{SRC} = E_c \tan\phi\langle -\epsilon_3\rangle, \tag{13}$$

where ϕ is the Coulomb's friction angle.

S is a scale factor introduced to provide a better correlation of the delamination area with the experiments.

The reader is referred to Material Science Corporation (MSC) and University of Delaware Center for Composite Materials[12] for a more detailed description of the material model.

MAT_162 also accounts for the effect of the strain rate by a logarithmic function on the strength and moduli properties, as defined respectively in Equations (14) and (15):

$$\{S_{RT}\} = \{S_0\}\left[1 + C_{\text{rate1}}\ln\left(\left\{\frac{\dot{\bar{\epsilon}}}{\dot{\bar{\epsilon}}_0}\right\}\right)\right], \tag{14}$$

where C_{rate1} is a material input parameter as defined in Table 3, $\{S\} = \{S_{aT}\ S_{aC}\ S_{bT}\ S_{bC}\ S_{FC}\ S_{FS}\}$ and $\{\bar{\epsilon}\} = \{|\varepsilon_1||\varepsilon_1||\varepsilon_2||\varepsilon_2||\varepsilon_3|(\varepsilon_{31}{}^2 + \varepsilon_{23}{}^2)1/2\}$.

$$\{E_{RT}\} = \{E_0\}\left[1 + \{C_{\text{rate1}}\}\ln\left(\left\{\frac{\dot{\bar{\epsilon}}}{\dot{\bar{\epsilon}}_0}\right\}\right)\right], \tag{15}$$

where $\{E\} = \{E_a\ E_b\ E_c\ G_{ab}\ G_{bc}\ G_{ca}\}$, $\{\bar{\epsilon}\} = \{|\varepsilon_1||\varepsilon_2||\varepsilon_3||\varepsilon_{12}||\varepsilon_{23}||\varepsilon_{31}|\}$, and $\{C_{\text{rate1}}\} = \{C_{\text{rate2}}\ C_{\text{rate2}}\ C_{\text{rate4}}\ C_{\text{rate3}}\ C_{\text{rate3}}\ C_{\text{rate3}}\}$.

The element is eroded when fiber tensile failure is predicted in both directions and the axial tensile strain is greater than E_LIMIT, or the compressive relative volume in a failed element is smaller than ECRSH, or the tensile relative volume in a failed element is greater than EEXPN. Also, an additional erosion criterion was added, using the card MAT_ADD_EROSION, to remove overstrained elements. In particular, the element is removed when the maximum effective strain is greater than 100% (EFFEPS = 1).

The material input parameters for Kevlar29/Epoxy are reported in Table 3.

MAT_162 is implemented for solid elements; therefore, constant-stress solid elements were used to mesh the panel. The standard LS-DYNA viscous-type hourglass control (IHQ = 1) was used, and the hourglass coefficient was QM = 0.1. The panel was modeled as a monolithic part and, by using the meshing technique explained in Material Science Corporation (MSC) and University of Delaware Center for Composite Materials,[12] the material model automatically detects delamination planes between each layer. In this way, there is a substantial reduction of contact interfaces and therefore of the computational cost of the simulation. It is preferred that each layer is represented by at least three element trough the thickness so that delamination, once it has occurred, is assigned to one third of the layer. For this reason,

the element dimensions were 1 × 1 × 0.148 mm where 0.148 was equal to one third to the average thickness of the layer. The numerical model implemented for MAT_162 is shown in Figure 1B.

3 | DISCUSSION

The results of the numerical models are compared with the experimental results in terms of the prediction of the ballistic curve, which was calculated fitting the data on the Recht-Ipson model.[27] The ballistic limit velocity was calculated as the intercept of the ballistic curve with the axis of abscissas (axis of impact velocity).

Regarding MAT_058, a parametric study on the value of SLIMT = SLIMT1 = SLIMT2 is shown in Figure 3A. The values of SLIMT equal to 0.05 and 0.1, which are at the extremes of the range recommended in the software manual,[25] yielded good result in terms of replication of the linear region of the ballistic curve (impact velocity higher than 430 m/s), but the baseline value of 0.1 yielded a better precision of the prediction of the ballistic limit velocity than the value of 0.05. A value of SLIMT of 0.2 is out of the recommended range and increases the energy absorbed by the composite material. For this reason, the predicted ballistic limit velocity was higher, and therefore, this prediction was more accurate, but the numerical model failed to replicate the linear region of the ballistic curve. In Figure 3B, the parametric study on the value of ERODS is reported. As defined in Section 2.1, this is the maximum effective strain for element erosion and must be chosen so that it does not affect the failure criterion and that the model is not polluted by overstrained elements.[26] By increasing this value, the ballistic curve is shifted rightward and downward, meaning that the energy absorbed by the composite material is increased. The most accurate prediction, considering both higher and lower impact velocities, was the baseline value of ERODS = 1.0.

The numerical model implemented with MAT_162 satisfied an acceptability limit of about 10% of the ratio of the hourglass energy over the total energy[28] for impact velocities of 430 m/s and higher. This energy check was not satisfied for lower impact velocities. Other viscous-type hourglass controls (IHQ = 2 and IHQ = 3) were tested, but they yielded higher hourglass energy than the standard LS-DYNA hourglass control (IHQ = 1). Also, stiffness-type hourglass controls available by the software were tested, but these hourglass controls are usually not recommended for high-velocity impact, and indeed, they did not lead to realistic deformation of the composite panel. A parametric study on the value of QM is shown in Figure 4A. By decreasing the baseline value of QM = 0.1 (which is the software standard value), the hourglass energy was slightly reduced while the accuracy of the prediction of the ballistic curve was also slightly reduced. Also, for the value of QM = 0.05, the hourglass energy check was not satisfied for impact velocities below 430 m/s. By increasing the value of QM, the hourglass energy was slightly increased, but, also in this case, the accuracy of the prediction of the ballistic curve was slightly worse. In Figure 4B, the parametric study on the value of EFFEPS is reported. As noted for Figure 3B, by increasing this value, the ballistic curve is shifted rightward and downward, meaning that the energy absorbed by the composite material is increased. The baseline value of EFFEPS = 1.0 led to better accuracy of the prediction of the ballistic curve.

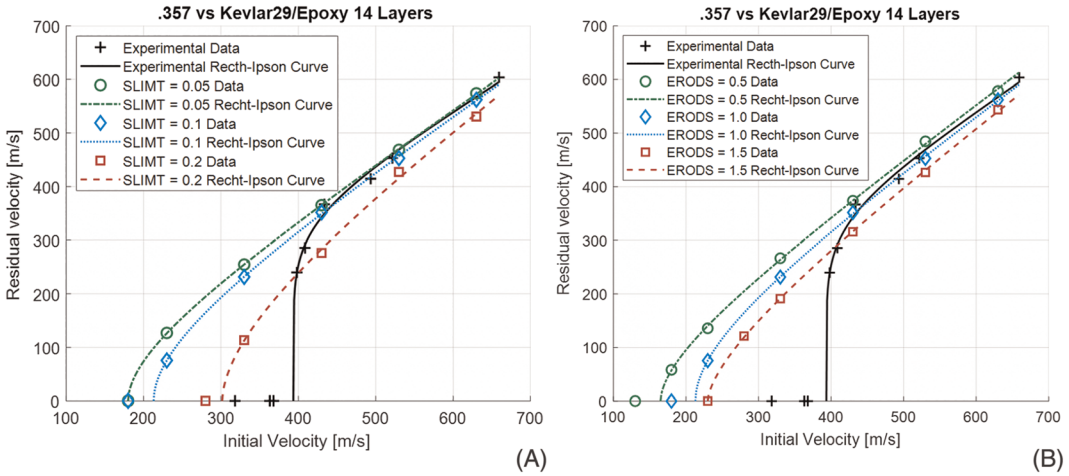

FIGURE 3 Parametric study on A, SLIMT = SLIMT1 = SLIMT2 and B, ERODS with MAT_058

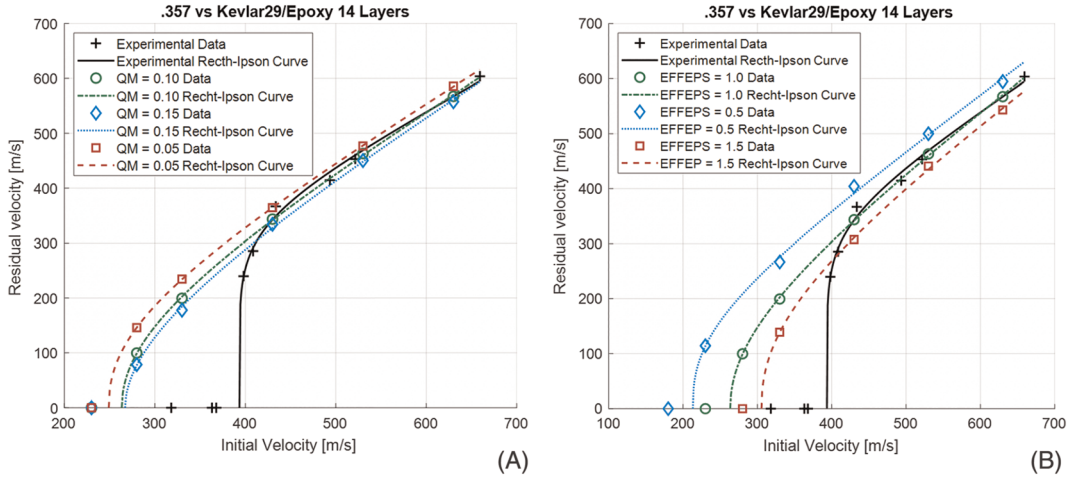

FIGURE 4 Parametric study on A, QM and B, EFFEPS with MAT_162

The baseline models with MAT_058 and MAT_162 are compared in Figure 5. Both numerical models were extremely accurate in replicating the linear region of the ballistic curve. Accuracy of the models was lower for impact velocities below 430 m/s approaching the ballistic limit velocity. In particular, MAT_162 was more accurate than MAT_058 since the error on the prediction of the ballistic limit was 33% for the former and 46% for the latter. The damage morphology of the two material models is compared in Figure 6: MAT_058 predicted more extended damage than MAT_162, the latter being more accurate in the reproduction of the experimentally observed damage morphology; furthermore, MAT_162 predicted a circular hole both in the front and the back face while MAT_058 predicted a less realistic hole of a rectangular shape. The numerical model with MAT_162 was more efficient due to the absence of all the contact surfaces between each couple of adjacent layers since the panel was modeled as one part. Consequently, the computational time was lower even if the number of elements was higher. In particular, the computational time for MAT_058 is around 2 hours, while it is around 1 hour for MAT_162 (using 4 MPP processors).

In conclusion, a mesh convergence analysis was performed as reported in Figure 7. Regarding MAT_058, the dimension through the thickness was kept always equal to 0.445 mm in order to always have only one element trough the thickness of each layer since it is not recommended to stack thick shell elements. Regarding MAT_162, the dimension through the thickness direction was kept always equal to 0.148 in order to always have three elements through the thickness of each layer. The other two dimensions were changed in a range between 2 and 0.25 mm. As shown in Figures 8 and 9, by decreasing the element size, the deformation of the panel decreases, and therefore, the energy absorbed decreases (especially considering MAT_162). This means that the ballistic curve is shifted upwards and leftwards as

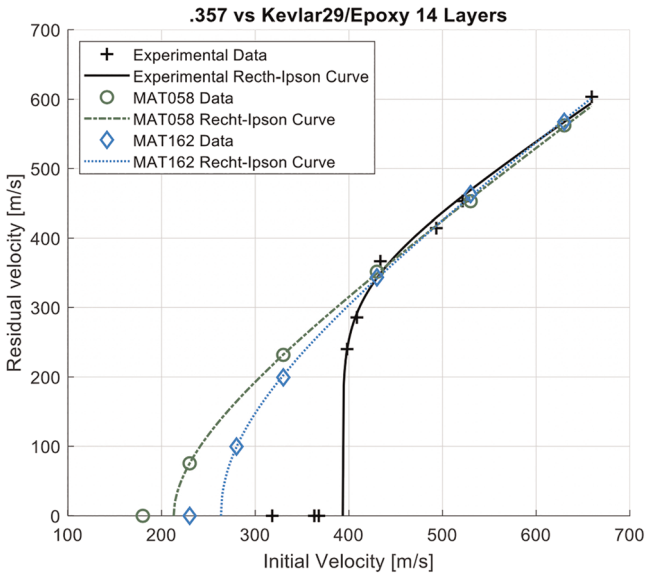

FIGURE 5 Comparison of MAT_058 and MAT_162 baseline models

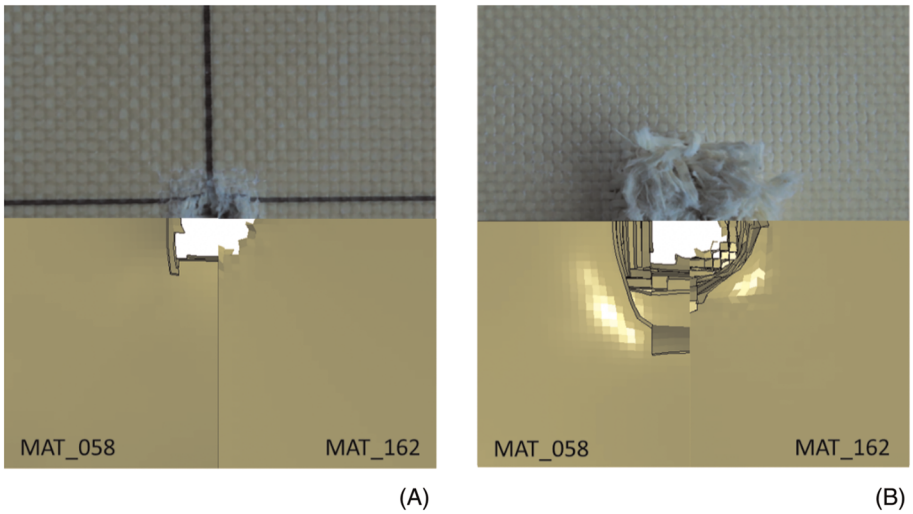

FIGURE 6 Comparison between experimentally observed and predicted damage morphology for A, front face and B, back face

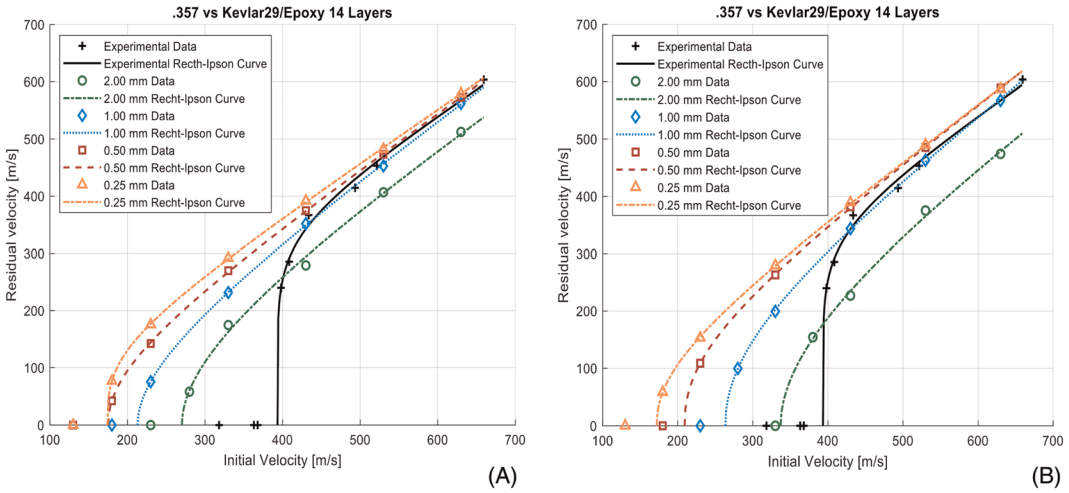

FIGURE 7 Mesh convergence analysis performed with A, MAT_058 and B, MAT_162

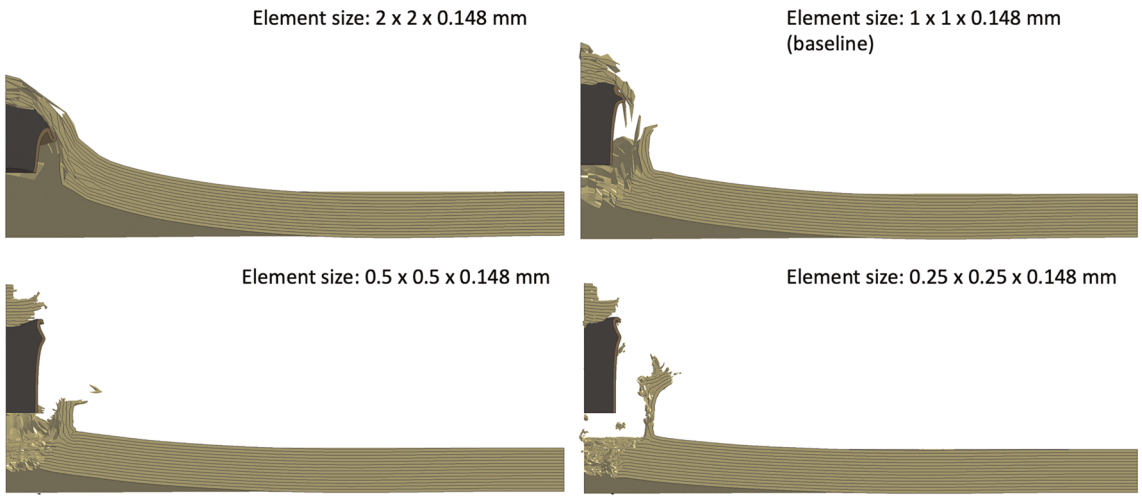

FIGURE 8 Effect of element size on the predicted deformation of the target with MAT_058

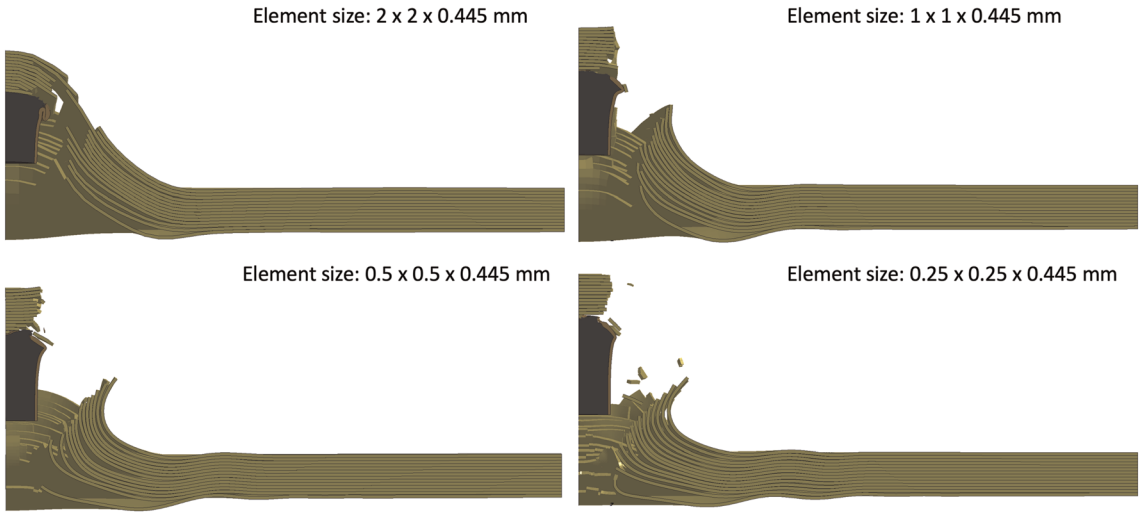

FIGURE 9 Effect of element size on the predicted deformation of the target with MAT_162

shown in Figure 7. Regarding MAT_058, while it seems that convergence is reached for the value of the ballistic limit velocity for an element dimension of 0.5 mm and smaller, at lower impact velocities, convergence of the residual velocity is not reached. Indeed, for an impact velocity of 180 m/s, the residual velocity is 42 m/s for 0.5-mm element dimension while it is 77 m/s for 0.25-mm element dimension. Regarding MAT_162, it seems that convergence is reached in the linear region of the ballistic curve for an element dimension of 0.5 mm and smaller, but this is not the case for the ballistic limit velocity, which decreases as the element dimension decreases without reaching a convergence value. The baseline element dimension of 1 mm led to better accuracy of the prediction of the ballistic curve.

4 | CONCLUSION

High-velocity impact on fiber-reinforced composites was simulated using the finite element method and using two different material models for the target: laminated composite fabrics (MAT_058) and composite MSC (in particular MAT_162). A parametric study of the parameters SLIMT1 and SLIMT2 and ERODS with MAT_058 and of the parameters QM and EFFEPS with MAT_162 was performed. MAT_162 showed more accuracy in the prediction of the ballistic limited velocity and lower computational time. Indeed, MAT_162 allowed to model delamination without the need of modeling each layer as a separate entity. This led to a lower number of contact interfaces and therefore a lower computational cost. MAT_162 was also more accurate in the reproduction of the damage morphology. Finally, mesh convergence analysis was performed. It was found that by decreasing the element size, the deformation of the panel decreases, and therefore, the energy absorbed decreases.

ACKNOWLEDGEMENT

Support by the Italian Ministry of Education, University and Research, through the project Department of Excellence LIS4.0 (Integrated Laboratory for Lightweight e Smart Structures), is acknowledged.

ORCID

R. Scazzosi https://orcid.org/0000-0002-1890-4724

REFERENCES

1. Mallick PK, "Fiber-reinforced composites: materials, manufacturing, and design," 2007.
2. Tham CY, Tan VBC, Lee HP. Ballistic impact of a KEVLAR® helmet: experiment and simulations. *Int J Impact Eng.* 2008;35(5): 304-318.
3. Gower HL, Cronin DS, Plumtree A. Ballistic impact response of laminated composite panels. *Int J Impact Eng.* 2008;35(9):1000-1008.

4. Manes A, Bresciani LM, Giglio M. Ballistic performance of multi-layered fabric composite plates impacted by different 7.62 mm calibre projectiles. *Procedia Eng.* 2014;88:208-215.
5. Li YQ, Li XG, Gao X-L. Modeling of advanced combat helmet under ballistic impact. *J Appl Mech.* 2015;82(11):111004-1–111004-9.
6. Bresciani LM, Manes A, Ruggiero A, Iannitti G, Giglio M. Experimental tests and numerical modelling of ballistic impacts against Kevlar 29 plain-woven fabrics with an epoxy matrix: macro-homogeneous and meso-heterogeneous approaches. *Compos Part B Eng.* 2016;88:114-130.
7. Scazzosi R, Manes A, Petrone G, Giglio M. Two different modelling approaches for fabric composites subjected to ballistic impact. *IOP Conf Ser Mater Sci Eng.* 2018;406:1–12. 012051.
8. Nunes SG, Scazzosi R, Manes A, Amico SC, de Amorim Júnior WF, Giglio M. Influence of projectile and thickness on the ballistic behavior of aramid composites: experimental and numerical study. *Int J Impact Eng.* 2019;132:1–13. 103307.
9. Berk B, Karakuzu R, Toksoy AK. An experimental and numerical investigation on ballistic performance of advanced composites. *J Compos Mater.* 2017;51(25):3467-3480.
10. Kumar S, Gupta DS, Singh I, Sharma A. Behavior of Kevlar/epoxy composite plates under ballistic impact. *J Reinf Plast Compos.* 2010;29(13):2048-2064.
11. Nayak N, Banerjee A, Panda TR. Numerical study on the ballistic impact response of aramid fabric-epoxy laminated composites by armor piercing projectile. *Procedia Eng.* 2017;173:230-237.
12. Material Science Corporation (MSC) & University of Delaware Center for Composite Materials (UD-CCM), "*A Progressive Comosite Damage Model for Unidircetional and Woven Fabric Composites*." 2017.
13. Gama BA, Gillespie JW. Finite element modeling of impact, damage evolution and penetration of thick-section composites. *Int J Impact Eng.* 2011;38(4):181-197.
14. Xiao JR, Gama BA, Gillespie JW. Progressive damage and delamination in plain weave S-2 glass/SC-15 composites under quasi-static punch-shear loading. *Compos Struct.* 2007;78(2):182-196.
15. Deka LJ, Bartus SD, Vaidya UK. Damage evolution and energy absorption of E-glass/polypropylene laminates subjected to ballistic impact. *J Mater Sci.* 2008;43(13):4399-4410.
16. Jordan JB, Naito CJ, Haque BZ. Quasi-static, low-velocity impact and ballistic impact behavior of plain weave E-glass/phenolic composites. *J Compos Mater.* 2014;48(20):2505-2513.
17. Li J, Huang C, Ma T, Huang X, Li W, Liu M. Numerical investigation of composite laminate subjected to combined loadings with blast and fragments. *Compos Struct.* 2019;214, no. November 2018:335-347.
18. Li XG, Gao X-L, Kleiven S. Behind helmet blunt trauma induced by ballistic impact: a computational model. *Int J Impact Eng.* 2016;91:56-67.
19. Scazzosi R, Manes A, Giglio M. Analytical model of high-velocity impact of a deformable projectile against textile-based composites. *J Mater Eng Perform.* 2019;28(6):3247-3255.
20. Rebouillat S. Tribological properties of woven para-aramid fabrics and their constituent yarns. *J Mater Sci.* 1998;33(13):3293-3301.
21. Gilioli A, Manes A, Giglio M, Wierzbicki T. Predicting ballistic impact failure of aluminium 6061-T6 with the rate-independent Bao–Wierzbicki fracture model. *Int J Impact Eng.* 2015;76:207-220.
22. Zukas JA, High Velocity Impact Dynamics. 1990.
23. Matzenmiller A, Lubliner J, Taylor RL. A constitutive model for anisotropic damage in fiber-composites. *Mech Mater.* 1995;20(2):125-152.
24. Schweizerhof K, Weimar K, Munz T, Rottner T. Crashworthiness analysis with enhanced composite material models in LS-DYNA—merits and limits. In: *LS-DYNA World Conference*; 1998.
25. Livemore Software Technology Corporation (LSTC), "*LS-DYNA Keyword User's Manual—Volume II—Material Models*." 2017.
26. Barauskas R, Abraitiene A. Multi-resolution finite element models for simulation of the ballistic impact on non-crimped composite fabric packages. *Compos Struct.* 2013;104:215-229.
27. Recht RF, Ipson TW. Ballistic perforation dynamics. *J Appl Mech.* 1963;30(3):384–390.
28. Chen X, "Advanced fibrous composite materials for ballistic protection," 2016.
29. Børvik T, Dey S, Clausen AH. Perforation resistance of five different high-strength steel plates subjected to small-arms projectiles. *Int J Impact Eng.* 2009;36(7):948-964.

How to cite this article: Scazzosi R, Giglio M, Manes A. Numerical simulation of high-velocity impact on fiber-reinforced composites using MAT_162. *Mat Design Process Comm*. 2020;e163. https://doi.org/10.1002/mdp2.163